ACS OMEGA

http://pubs.acs.org/journal/acsodf

Article

Crystallographic Pattern Mediates Fungal Nanoadhesion Bond Formation on Titanium Nanotubes

Benjamín Valdez-Salas,* Ernesto Beltrán-Partida,* Mario Curiel-Álvarez, Minerva Guerra-Balcázar, and Noé Arjona

Cite This: *ACS Omega* 2021, 6, 15625−15636

Read Online

ACCESS | Metrics & More | Article Recommendations | Supporting Information

ABSTRACT: The development of nanoadhesion bonds at the cell−material biointerface has been considered as a current prospective mechanism of microbial adhesion and colonization. However, there is a tremendous lack of evidence for the rational design of outstanding antifungal nanoconfigured materials. Therefore, extending our previous insights of evidence, we found that blocking the adhesion and biofilm formation of *Candida albicans* on NTs requires the inhibition of fungal nanoadhesion bonds. This work reports a concept for understanding the antifungal behavior of the crystallographic phase for anatase (NTs-annealed) and amorphous NTs. Herein, we demonstrated that the crystallographic orientation is a predominant parameter to reduce *C. albicans*, over the surface roughness and chemistry. We showed that the anatase phase conducted to an invasive phenotype, cellular envelopment insertion, followed by the improved cellular spread. Meanwhile, the amorphous configuration imposed reduced nanoadhesion bonds mainly appreciated over the mouths of the NTs, as revealed by cross sectioning. Moreover, our results showed that under fungal conditions, the experimental materials could reduce the surface energy. This work highlights that the crystallographic pattern predominantly controls the antifungal activity of NTs. The evaluated systems proposed that the NTs-annealed conducted an optimized insertion of fungal cells. Nonetheless, amorphous NTs inhibited the deposition of *C. albicans* via blocking the insertion and the development of nanoadhesion bonds, without morphology aberrations. The present discoveries can further inspire the rational design of upgraded nanoconfigured surfaces with noteworthy antifungal characteristics for antimicrobial coating technologies.

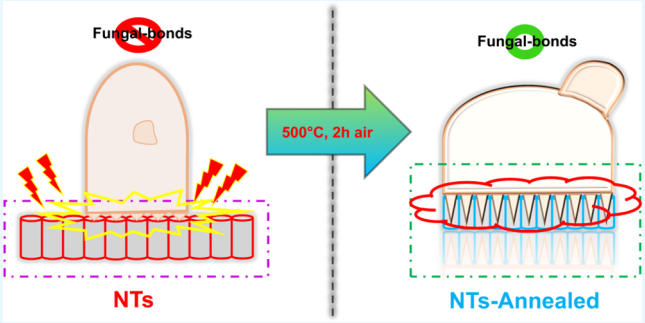

INTRODUCTION

Microbial colonization of medical devices and implant surfaces is an important issue that consequently affects the biomaterial implantable systems' healing and success.[1] The resulting microbial growth process mainly characterized in failure implants has followed a subsequent cellular adhesion course governed by the deposition of microbial macromolecules.[2] Moreover, in order to sustain the microbial adhesion, it is strongly required to form electrostatic interactions at the cell−material interface that promotes the initial nanocontact to biomaterial surfaces.[2,3] Thus, after the adhesion, a continuous microbial proliferation will be succeeded by expansion of the generation of biofilm sensing molecules, which mostly leads to a mature colonization.[4,5] Far more critical, *Candida albicans* is the leading fungal agent associated with a vast number of concurrent biomaterial-related infections.[6,7] Of particular concern, the growth biology of *C. albicans* is similar to that required for infectious biofilms, which strongly suggests that it entails a well-conducted preliminary surface attachment in order to succeed as a matured consortium.[2,5,8] Despite strict clinical pharmacological protocols for managing infectious diseases, the current microbial resistance is another substantial damaging threat for any particular medical procedure.[9,10] Importantly, the presence of fungal cells (e.g., *C. albicans*) is the whole platform to orchestrate multiple microbial consortium formation (microcosm). Thus, collectively, the existing antifungal chemotherapies fairly fail to avoid the adequate adhesion and microcosm formation of biofilms by essential fungal cells. Therefore, considering the upsetting consequences of microbial adhesion, it is urgently demanded to develop outstanding antimicrobial strategies that detriment the initial microbial−surface attachment interactions at the nanoscale on implantable systems.

To counteract the microbial adhesion, several synthetic improvements have been developed on biomaterials by

Received: January 26, 2021
Accepted: May 26, 2021
Published: June 8, 2021

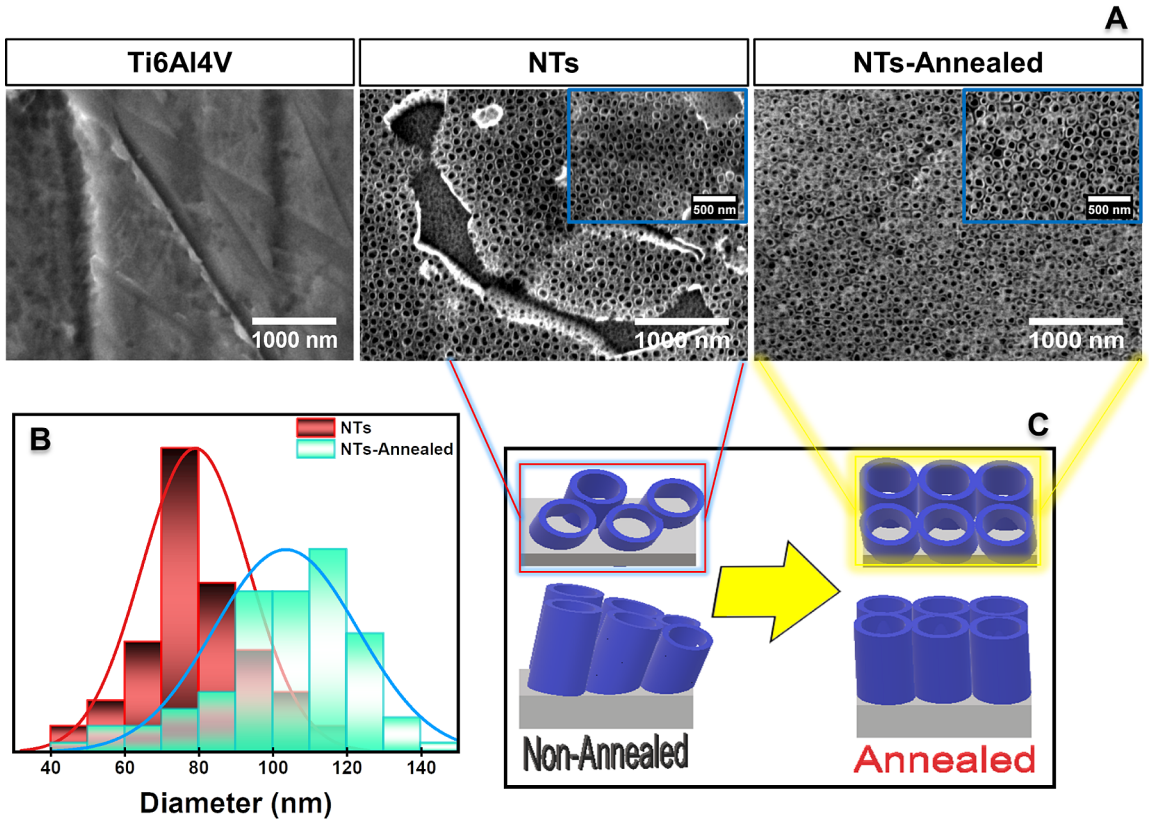

Figure 1. FE-SEM characterization of the experimental materials. (A) Surface morphology showing the presence of NTs over the anodized materials and the control alloy. The insets represent the high zoom of the NTs. (B) Diameter distribution of the as-prepared and annealed NTs. (C) Schematic illustration of the NT coating representing a molecular rearrangement because of the annealing process.

conducting nanoroughness surface modifications,[6,11,12] functionalization with antimicrobial agents,[13,14] chemical and crystallographic transformations,[15,16] and nanopattern architecture fabrication.[7,17] However, most of the antimicrobial modifications can lead to critical side effects on mammalian cell, resulting in extensive failure of the surface materials.[18−21] A promising and imperative strategy to develop antimicrobial repellent surfaces is based upon the rational design of engineered surfaces that point toward the important high aspect ratio, which hallmarks the nanoconfiguration. The application of nanostructured surfaces can promote successful cellular growth for tissue regeneration.[22,23] Meanwhile, it could further detriment the fungal cell attachment and biofilm formation by limiting the establishment of effective nanoadhesion bonds.[24] Nonetheless, a critical concern of the microbial adhesion studies evaluating the relationship between surface physicochemical parameters is that they are only limited to the role of bacterial models. It is noteworthy to highlight that further supporting investigations are urgently required to assess the knowledge gap behind the fungal phenomenon involving the cell−material nanoscale bonding process.

Previously, we described the fungal adhesion on the as-manufactured anodized NTs (amorphous phase) fabricated on the Ti6Al4V medical alloy surface against a flat control, proposing that the surface patterns regulate the early formation of nanoadhesion bonds.[24] Importantly, the NTs promoted a higher surface roughness, which in part generated an increased spatial distance between NT surface valley peaks, thus disturbing the contact bonding of the fungal-wall surface. Earlier microbial adhesion works have suggested that the elevated energy interactions resulting from increasing the nanoroughness could interrupt the close contact interplay required for the proper cell binding.[6,11] Moreover, the high stiffness provoked by NTs led to the formation of suppressed contact points, further proposing that homogeneous NTs dramatically disrupt the initial attachment process of *C. albicans*.[24] Importantly, the biofilm formation ability was avoided, as proposed in previous works of bacterial adhesion on nanostructured Ti-based materials.[25] Thus, these findings have stimulated the fabrication of controlled nanostructured surfaces on Ti6Al4V for the continuous mitigation of the fungal adhesion.[7] Nonetheless, previous studies have advocated that the transformation of NTs by thermal annealing to the anatase configuration (NTs-annealed) can notably optimize the biocompatibility and wettability of NTs.[26] However, there is no consensus describing the fungal repellent capability behavior on NTs-annealed, thus resulting in a lack of evidence of antifungal activity. Previous works of bacterial adhesion have proposed that wetter and crystallographic-ordered Ti surfaces can promote the bacterial adhesion and susceptible biofilm invasion.[15,27−29] Therefore, it is firmly required to advance the understanding of the relationship between the surface crystallinity and the fungal attachment regulation by the formation of nanobonding.

The present study investigates the role of the as-manufactured and anatase-phase NTs in the formation, growth, and control of nanoadhesion bonds (demanded for biofilm formation) to advance our knowledge in the design of antifungal and repellent material surfaces. Therefore, we

https://doi.org/10.1021/acsomega.1c00475
ACS Omega 2021, 6, 15625−15636

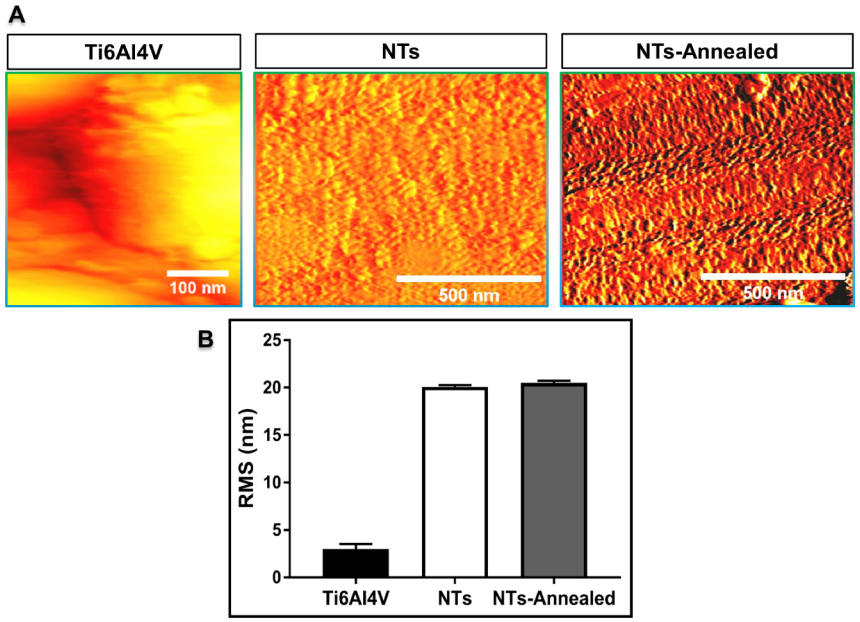

Figure 2. Surface topography of the materials. (A) Representative AFM micrographs of the Ti6Al4V materials for each corresponding process. (B) RMS quantitative evaluation.

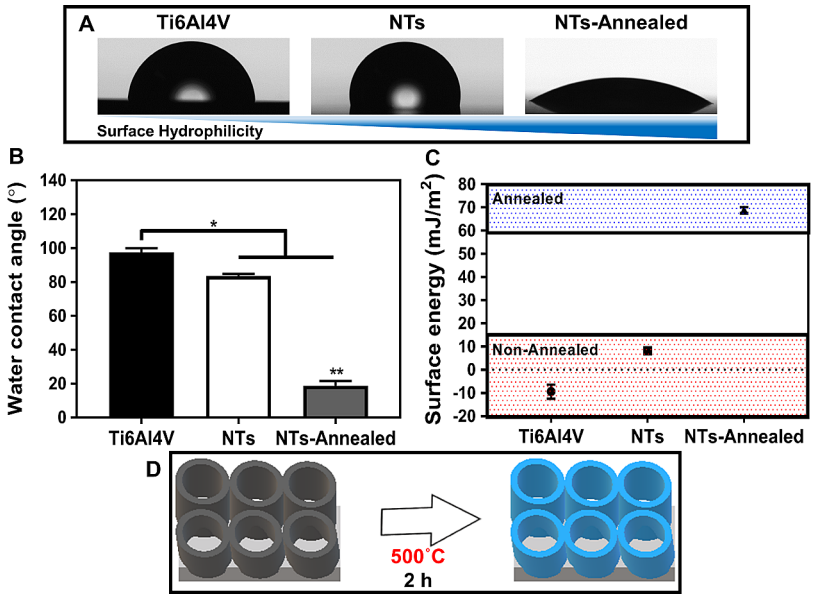

Figure 3. Wettability of the experimental materials. (A) Waterdrop morphology after 5 s deposited on the materials. (B) Static contact angle measurements. (C) Surface energy analyses. (D) Schematic illustration of the transformation from hydrophobic to hydrophilic NTs. The * and ** indicate significant differences.

fabricated NT samples with constant roughness magnitudes and chemical profiles for validating the involved adhesion mechanism. Importantly, *C. albicans* was cultured over the experimental materials to analyze the adhesion, viability, morphology, and in the improving of wetting effect on biocompatible surfaces. Our results open up a new road for designing and evaluating active biological surfaces for medical, dental, biomedical, and industrial applications.

RESULTS

The specific morphology of the anodized and thermally annealed nanopatterned materials was characterized using high-resolution field emission scanning electron microscopy (FE-SEM), as represented in Figure 1. Initially, we can describe that our standard anodization process resulted in the formation of the well-defined NTs (Figure 1A). Moreover, the annealing process did not alter the nanotubular architecture orientation among the substrate surface. In this regard, it is imperative to indicate that the diameter distributions were 79 ± 4 and 83 ± 9 nm after the annealing process (Figure 1B), without significant changes as anticipated. Importantly, by applying high amplification of the annealed samples, we detected that the nanotubular construction substantially showed a continuous sharpened nanoedges, as illustrated in Figure 1C. Moreover, the NT lengths were of 400 nm.[30] However, the polished control surface showed a flat morphology, as expected. The surface chemical composition

https://doi.org/10.1021/acsomega.1c00475
ACS Omega 2021, 6, 15625−15636

of each experimental procedure was characterized by energy-dispersive X-ray spectroscopy (EDX) (Table S1). Interestingly, the control alloy surface was prominently constituted by Ti (86.05%), with Al (6.26%), V (4.11%), and C being the lower-grade elements. In contrast, the nanostructured surfaces illustrated projecting outcomes of increased oxidation. Therefore, it is considered that the anodization promotes a thick formation of a controlled and orientated oxide layer[26,30] and the following annealing process under air conditions improves this oxidized coating layer. It is firmly congruent that the NTs-annealed showed a higher O (36.7%) composition than the NT model (20.32%). The Al levels were found to be 4.06% (NTs), which are mutually similar to those of NTs-annealed (4.14%). A substantial chemical insight was that the F element of NTs was not detected in the annealed nanostructures, as suggested in previous works.[31]

The topography configuration of a material surface dictates part of the biological behavior, mainly acting as a sensor for the microbial adhesion; thus, the roughness of the substrates was studied by atomic force microscopy (AFM), as shown in Figure 2. The surface topography differences are clearly presented in Figure 2A, indicating that the anodization process resulted in the nanopatterning of the Ti6Al4V substrates. Similarly, the NTs-annealed illustrated a conserved rougher topography, as pictured in the NTs. Importantly, the 3D analysis of the nanostructures indicates that homogeneous and continuous pore-like structures were patterned over the surfaces (Figure S1). In contrast, the control material results in a flat structural topography (Figure 2A), agreeing with the FE-SEM (Figure 1A). The roughness quantification for each experimental surface was provided as the root-mean-square (RMS) numerical data, indicating that the annealing process did not result in a consistent roughness modification (Figure 2B). However, as proposed, the control Ti6Al4V-polished surface outlined a significantly reduced roughness throughout the regular flat surface (Figure 2B).

The wetting properties of the synthesized materials were evaluated using the water contact angle (WCA) (Figure 3). The droplet morphologies captured using a high-resolution camera (Figure 3A) evidently shows that the surface modifications increased the wettability properties. Moreover, the analytical characterization illustrated a significantly reduced WCA for the nanoimproved materials, highlighting a super-wettability performance for the NTs-annealed model (Figure 2B). Similarly, the electrochemical modification promotes higher surface energy values, and they increase again after the annealing process (Figure 2C). However, Figure 3D illustrates a schematic representation of the hydrophilicity achievement after applying the annealing process, which, as discussed in previous works,[26] firmly reduces the water repellent performance. In Figure 4, the X-ray diffraction (XRD) pattern orientation of the nanostructured materials is shown. The as-anodized NTs showed the outcomes of a completely amorphous oxide coating layer, only illustrating diffraction peaks corresponding to the Ti bulk material, as expected. Nonetheless, the thermal protocol influenced the crystal structure of the oxide coating, depicting the characteristic anatase lattice peaks (Figure 4, red line).

The development of antimicrobial surfaces, principally antifungal coatings for biomedical applications, is a current imperative requisite for the success of implant materials. Therefore, we evaluate the initial fungal viability conducted by the engineered substrates (Figure 5). It is important to

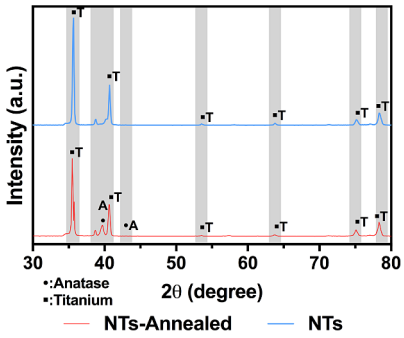

Figure 4. XRD patterns of the as-anodized and annealed NTs.

postulate that we consider two fungal adhesion phases for the systematic cellular behavior evaluation in this study: 2 h as an initial adhesion and 6 h as a late adhesion phase. In Figure 5A, the recovered cellular growing colonies from the experimental materials are represented. Moreover, after 2 h of incubation, we did not detect significant differences in the fungal viability (Figure 5B). However, at 6 h, it was remarkably observed that the Ti6Al4V alloy surface allows a higher late fungal adhesion. Furthermore, the NTs-annealed showed better fungal colonization than the NTs (amorphous phase). Importantly, the NTs suppressed the active fungal growing performance, and even they were comparable with the experimental substrates in the initial adhesion phase (Figure 5B). However, Figure 5C compares the fungal adhesion viability relationship at 6 h and the roughness parameters for each experimental material. The results point that the surface roughness did not directly influence the late adhesion behavior on the nanopatterns, as a concerning difference can be highlighted among the NTs and their thermally treated counterparts (Figure 5C). In contrast, the control alloy (flatter surface) allowed increased outcomes of fungal colonization. In order to support the experimental results, we explored the interesting wetting behavior ability that conducted *C. albicans* over the experimental materials (Figure S2). Therefore, a suspension of *C. albicans* was prepared for sessile drop analysis, deposited, and analyzed on the surface of the experimental substrates. The presence of *C. albicans* increased the hydrophobic properties of the NTs, thus inversely decreasing the surface energy of the nanotubes (19.37 ± 4.21 mN/m). On the contrary, the Ti6Al4V substrate shows an increased hydrophilic behavior, suggesting that the presence of fungal cells enhanced the surface energy (38.36 ± 2.53 mN/m). Far more concerning, the NTs-annealed showed a strikingly significant increased surface energy (55.64 ± 3.54 mN/m), though presenting lower surface energy as observed previously (Figure 3B,C). Importantly, the fungal surface charge was determined from the ζ potential, resulting in 12 ± 3 mV.

The colonization of *C. albicans* on the experimental substrates was evaluated using FE-SEM at 2 and 6 h of culture (Figure 6). The control witnessed higher cellular colonization at 6 h in comparison with the 2 h on the control alloy, which was consistent with the viability results (Figure 5B). However, the nanostructured surfaces did not allow the early and late adhesion of *C. albicans*. Interestingly, the nanopatterns showed reduced outcomes of microbial growth when compared with the control alloy. Nonetheless, early results of fungal adhesion were clearly more notable on the NT-annealed surfaces compared to those of on NTs (amorphous). Similarly, after 6 h (late adhesion), an outstanding *C. albicans* growing ability

https://doi.org/10.1021/acsomega.1c00475
ACS Omega 2021, 6, 15625−15636

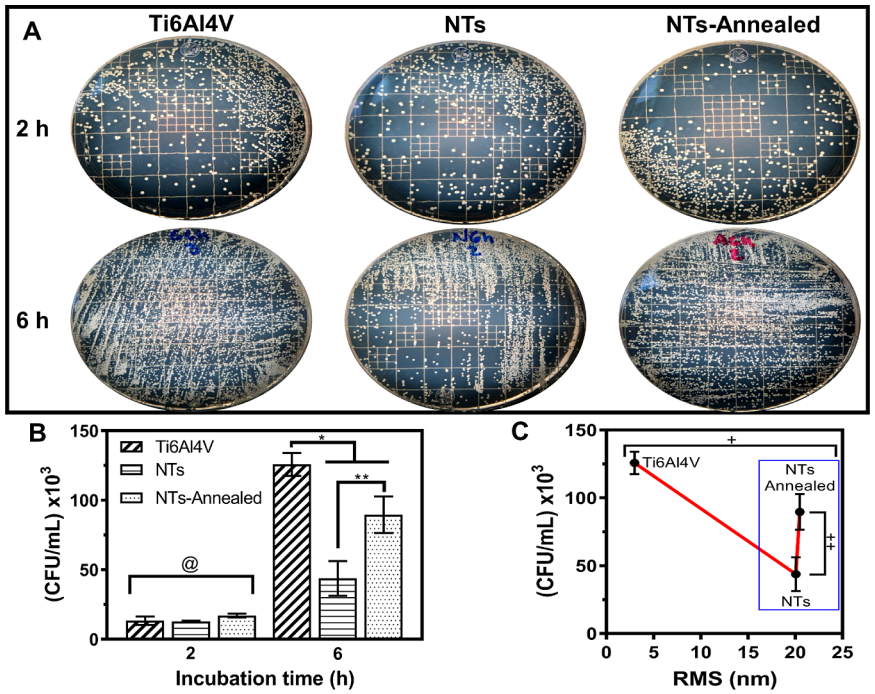

Figure 5. *C. albicans* assessment at each culture period. (A) Representative cell culture plates showing the decreased fungal growth on the NTs. (B) Quantitative analysis of the fungal viability of the materials. (C) Relationship between surface roughness and the fungal viability. The *, **, +, ++, and @ represent significant differences. The blue square highlights the nanostructured specimens.

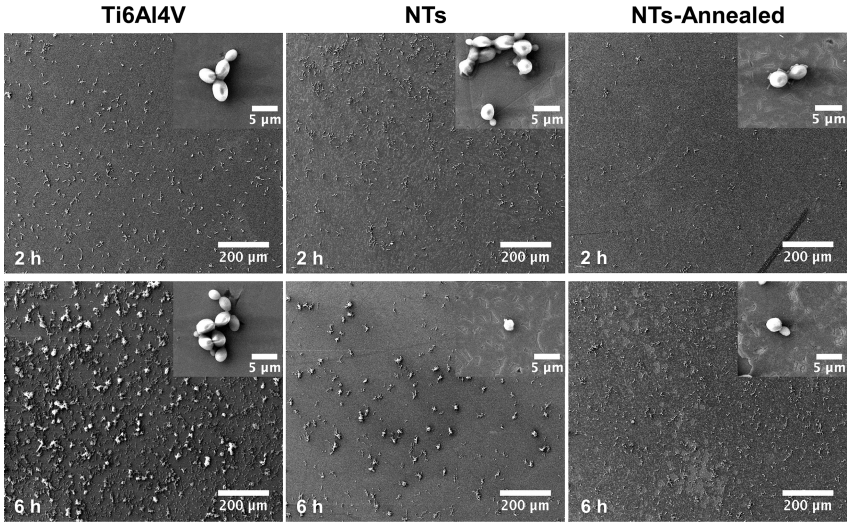

Figure 6. Representative FE-SEM micrographs of adhered fungal cells on the experimental surfaces after 2 and 6 h. The inset illustrates the cell-group arrangements.

was detected on the thermally fabricated materials, thus demonstrating the results of amplified fungal progression. Furthermore, the NTs consistently reduced the fungal viability (Figure 5A,B), taking together the ability to prohibit not only the required early adhesion phase but also, far more importantly, the continuing late adhesion need for successful colonization (Figure 6). However, the yeast phenotype expression on the materials revealed important structural modifications after each adhesion process (Figure S3). The control surface resulted in a well-defined ovoid morphology, with subsequent pseudohyphae formation at each adhesion period strongly suggesting hyphae development. Moreover, the early adhesion stage of NTs-annealed induces structural pseudohyphae formation, with a consequent yeast morphology similar to those observed for the control alloy. In addition, the late stage showed partial detrimental outcomes because of disrupting edges at the cell-wall surface (Figure S3, yellow arrows). In contrast, the NTs advocate the formation of a closed circular structure (altering the ovoid typical form), including a minuscule blastopore-like phenotype at 2 h of incubation. However, in the late adhesion, we detected strikingly structural abnormalities characterized by a distinctive, aberrant architecture, with an outstanding altered cell-wall disruption, suggesting cell lysis, utterly different from classical morphologies (Figure S3).

In Figure 7, we presented high-resolution magnified FE-SEM micrographs illustrating the contact adhesion and morphology configuration after 2 h of incubation. Initially,

https://doi.org/10.1021/acsomega.1c00475
ACS Omega 2021, 6, 15625−15636

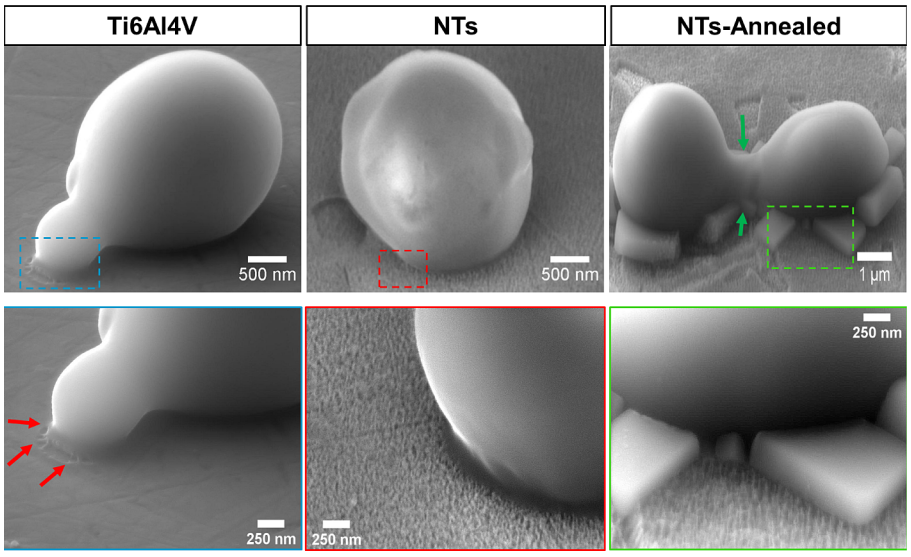

Figure 7. High-resolution tilted FE-SEM micrographs showing the adhesion differences conducted by the material specimens after 2 h. The dashed square lines represent the zones of higher magnification for the analysis of the cell-contact interactions. The red arrows indicate cellular interaction points. The green arrows point to the yeast septum formation.

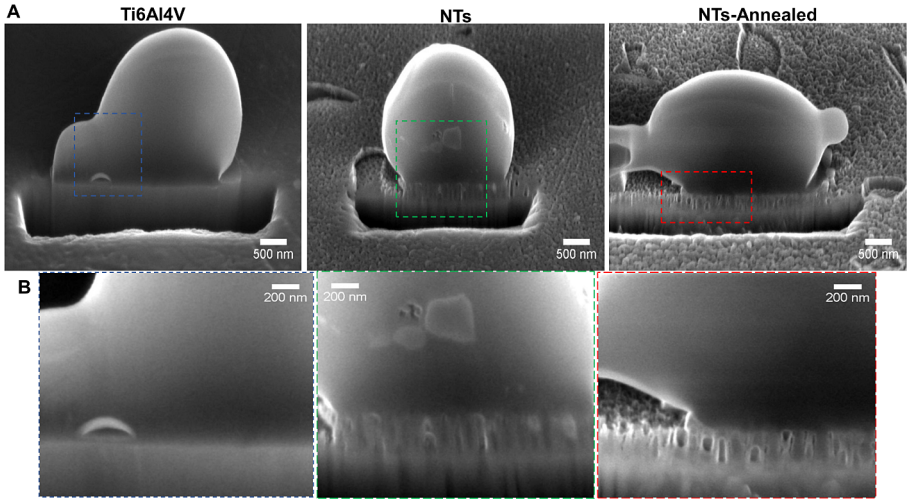

Figure 8. Nanoscale contact bonds at the fungal−material biointerface after 2 h of incubation. (A) Cross-sectional analysis by FIB milling exposing the adhesion behavior over the experimental materials. (B) High-magnification of the biointerface revealing the *C. albicans* nanocontact bonding interactions with the surface substratum, highlighting the inner envelope penetration on NTs-annealed.

the Ti6Al4V alloy control resulted in the development of contact points over the flat surface. Moreover, we can highlight that the control surface showed the formation of cellular fibril protrusions (Figure 7, red arrows), which could support a higher adhesion capability, as previously observed. Furthermore, the nanostructured materials led to different cellular morphologies. Interestingly, the NTs showed a yeast-like morphology; however, the high magnification resolved a rough surface morphology, diverging from those of the control alloy. This information may suggest that the *C. albicans* were facing difficulties establishing a correct invasion morphology in the early adhesion phase. Furthermore, we detected that *C. albicans* generated a reduced contacting surface area compared to the NTs-annealed and the control material. However, the annealed nanostructures showed a cell−cell connection status, highlighting the formation of a septum bonding between the cells (Figure 7, green arrows). Furthermore, despite the cell−cell bonding development, the *C. albicans* did not show hyphae formation but conserved a truly ovoid organization. However, they formed a stable basal layer, which could be constituted by exopolysaccharide substances secreted under the cells and crystal-like structures that could be associated with the salt precipitation from the culture medium and the PBS, as depicted by the high-magnified micrograph (Figure 7, green square).

To study the biointerface connecting the materials and *C. albicans* after 2 h of incubation (early adhesion), we used focused ion beam SEM (FIB-SEM). It is essential to postulate that the FIB milling process generates detailed cross sections of selective individual cells, which provides evidence of the bonding adhesion interactions occurring at the nanoscale fungal−material interface (Figure 8). A close inspection of the FIB-SEM micrographs illustrated that the early-stage phase showed a distributed deposition of *C. albicans* on the entire flat surface. Similarly, the FIB notably showed that the cells occupy a higher surface area of ≈3.24 μm in length/cell, which allowed

https://doi.org/10.1021/acsomega.1c00475
ACS Omega 2021, 6, 15625−15636

a considerable cell−surface interaction expanding the ability to cover the flat topography (high-zoom blue dashed square). Moreover, the NTs-annealed revealed a shorter cellular deformation (≈2.42 μm/cell in length) than those detected on the control alloy, suggesting that the nanopatterning may interrupt the cell spreading on the nanostructured surface. Importantly, high-magnification FIB milling at the interface revealed that the fungal envelope was deformed as following the NT orientation (high-zoom red dotted square). In the magnification, it can be resolved that the fungal wall was capable of penetrating the NTs, thus illustrating the insertion of individual membrane-wall component pattern nanobonds forcing the cell to anchor over the thermally nanostructured coating. Interestingly, the milling exposed the cell−cell interactions, also proposing that the surface may promote cellular communication. On the contrary, the NTs (amorphous) presented a reduced cellular distortion of ≈1.92 μm/cell in length, notably lower than the experimental materials. However, the cell height is higher than those of the NTs. The interface also highlights that the fungal membrane protrusions could not insert inside the NTs (Figure 8, high-zoom green dotted square), only generating reduced nanoadhesion bonds directly interacting with the nanotube mouths. Furthermore, the cross sectioning reveals that the phenotypic architecture was remarkably ovoid, which may suggest a repellant ability of the NTs, without the presence of pseudohyphae or cell−cell interactions.

DISCUSSION

Implant-associated infections have been widely described as occurring due to failure of medical devices, mainly concluding with the material replacement and its subsequent loss.[1] Interestingly, most of these infectious processes are closely related to bacterial adhesion and biofilm formation. Consequently, the major consensus of antimicrobial surface designs has focused on bacterial biology without including different species. However, recent studies show that fungal cells (e.g., *C. albicans*) play an important role as the principal cellular template for the proper bacterial adhesion and growing biofilm formation,[10,32] several of which require the rational design and development of next-generation antifungal surfaces. However, elucidating the underlying mechanisms governing the antifungal ability of nanostructured surfaces is critical for improving material performance. Therefore, here we evaluated the antifungal role of NTs in the anatase and amorphous phase, paying special attention to the crystallographic orientation effect in the *C. albicans* behavior. To advance our knowledge in the design of nanopatterned antifungal coatings, the NTs mainly differed in the crystallographic patterning; meanwhile, the size and roughness parameters were maintained constant. Interestingly, previous studies of bacterial adhesion have suggested that Ti nanorougher surfaces could disturb the required cell-binding interactions by provoking increased cellular elastic forces, resulting in cell rupture and death.[33−35] Previously, our group has described the capability of amorphous NTs to inhibit the adhesion of *C. albicans* by disrupting the formation of fungal adhesion bonds at the nanoscale.[24] Our present work indicates that the transformation of NTs to anatase did not significantly alter the tube diameter, therefore allowing the elucidation of the role of the anatase pattern in the conduction of fungal adhesion.

The surface chemical properties play a vital role in the promotion of bactericidal activity of nanostructured materials.[20] Similarly, previous studies have proposed surface chemical functionalization with antibiotics, metals, and more, to accomplish an effective, durable antimicrobial activity.[13,36,37] However, these surface modifications can show gradual ineffectiveness and, more importantly, a potent cytotoxic effect.[21] Therefore, we evaluated the chemical composition of materials, thus indicating that the substantial differences between the nanomaterials were a reduction in the fluoride levels from 2.91% (NTs) to nondetectable values (NTs-annealed). On the contrary, the oxygen content on the NTs increase from 20.32% (amorphous) to 36.7% (anatase), proposing the development of an ordered, thicker, and dense oxide layer. Although these dissimilarities could initially indicate a direct significant chemical difference, it is important to highlight that these fluoride levels may severely influence the bacterial adhesion instead of fungal attachment.[38,39] Hence, our results point toward those NTs that did not demonstrate relevant surface chemical discrepancies in the characterization of the fungal-nanotextured interactions.

Our AFM and 3D topography analysis revealed that the nanotextured materials maintained similar roughness values together with an ordered topography arrangement (Figures 2 and S1). Importantly, a wide number of studies suggest that the surface roughness was crucial in conducting the bacterial adhesion;[11,12,40] concernedly, the role of fungal cells is far still poorly understood. Interestingly, Le et al. characterized the influence of Ti surfaces textured with different nanoroughness magnitudes in the colonization of *C. albicans*.[6] The authors proposed that flat Ti surfaces (RMS 25.7 ± 8.5 nm) promoted similar *C. albicans* viable levels compared to nanorough Ti (484.0 ± 15.6 nm), after 24 h. Nonetheless, the polished Ti transformed the cells to a pseudohyphae phenotype, in which the nanorough Ti showed a yeast ovoid morphology,[6] as detected here. However, our work indicates similar outcomes of fungal viability on the substrates in the early adhesion stage (Figure 5B). However, after 6 h, the NTs overcome the antifungal activity, followed by the annealed NTs, and, finally, the Ti6Al4V control. Taken together, the relationship between the roughness and the *C. albicans* viability depicted that the topography did not directly influence the reduction of viable cells (Figure 5C). Substantially, our work highlights that the crystallographic patterns of nanotubular TiO_2 influence as a cornerstone in the cellular attachment, instead of the surface roughness and similar nanotube diameter. In a previous study, Almaguer-Flores et al. compared the bacterial adhesion behavior on magnetron sputtered crystalline and amorphous TiO_2 coatings.[41] The results illustrated lower *Escherichia coli* and *Staphylococcus aureus* adhesion on amorphous TiO_2 surfaces, despite the surface energy, chemical composition, and topography parameters remained constant, thus revealing a surface crystallinity control in the fungal adhesion fate. Inherently, further investigations are recommended to elucidate the specific mode of action corresponding to each physical parameter.

A significant increase in NT hydrophilicity after transforming to the anatase phase has so far been reported.[26] Similarly, previous works have proposed that anatase NTs could negatively encourage the bacterial attachment behavior. However, to the limit of our knowledge, this is the first study comparing the fungal adhesion behavior on anodized amorphous and anatase NTs. Here, we detected that the NTs-annealed increase the hydrophilic behavior compared to the counterpart NTs (Figure 3), probably by the improved

https://doi.org/10.1021/acsomega.1c00475
ACS Omega 2021, 6, 15625−15636

photocatalytic activity developed by the anatase phase.[42] Nonetheless, after characterizing the wetting properties of the experimental materials in contact with *C. albicans*, we detected that the Ti6Al4V control alloy improves its hydrophobic properties (Figure S2). However, the nanostructured materials showed a decreased wetting behavior in the fungal environment, resulting in a substantial hydrophobic divergence compared to the NTs-annealed. Interestingly, *C. albicans* exhibited a partial hydrophilic activity, thus outlining a positive ζ potential of 12 ± 3 mV. Furthermore, the NT anatase promoted an elevated energy wide band gap state (3.26 eV) compared to amorphous NTs,[43,44] resulting in remarkable enhanced electrical and catalytic properties.[45] Moreover, Gongadze et al. suggested a mathematical model supported by experimental evidence that considers the electrical field concentration at highly curved crystallographic edges that can modify the protein adsorption pattern.[46] Thus, in part, this effect may improve the adhesion behavior of *C. albicans* on NTs-annealed. From a chemical point of view, the anodization and thermal treatment may result in the formation of Ti^{3+} species, which has been attributed to a higher conductivity characterized by the formation of surface states that facilitate charge transfer.[47] Collectively, the increased wettability obtained by the cleaning process, which in turn results from the thermal treatment, may further act as a platform for the formation of promoted electrostatic interactions among the NTs-annealed and the fungal cells. Simultaneously, the heightened aspect ratio provided by the NTs-annealed and the underlying area available for electrostatic interactions could be retroactively supported. Hence, these hallmark properties may in part explain the extensive cellular deformation, the establishment of nanoadhesion bonds, and the observed fungal envelope penetration inside the NTs-annealed. Meanwhile, NTs highlighted a repellent behavior characterized by an abrupt cellular spreading and reduced nanoadhesion bonds mainly contacted with the NT mouths. Furthermore, the adhesion configuration analyzed from the FE-SEM results indicated that the control alloy developed a higher fungal−surface biointerface. Therefore, the NTs-annealed showed a higher *C. albicans* extension than NTs, proposing that the surface energy, the promoted band gap state, and elevated surface area may lead to an optimal cellular adhesion. In a previous study, it was demonstrated that oxygen-deficient zinc oxide nanowires (ZnO-NWs) presented antimicrobial efficacy against a fluconazole-resistant *Cryptococcus neoformans* (*C. neoformans*) model.[48] Interestingly, the authors suggested that the ZnO-NWs promoted a cellular stretched, deflected, with a spreading membrane morphology resulting in fungal leakage. Collectively, the FIB analyses supported that *C. neoformans* could not form nanoadhesion bonds,[48] which is in agreement with our results. However, it was reported that dragonfly nanostructured wing surfaces coated with a gold layer were capable of improving the death rate of *Saccharomyces cerevisiae* (*S. cerevisiae*). The FE-SEM results proposed a wide cell-wall mechanical disruption associated with a promoted cellular adhesion and a striking insertion of the fungal envelope.[49]

Previously, Bhadra et al. suggested a modest viability reduction of *Pseudomonas aeruginosa* and *S. aureus* on Ti NW surfaces fabricated by hydrothermal treatment.[34] The authors speculated a resulting cell-membrane deformation, which concluded with the cell rupture. Moreover, Ivanova et al. proposed that the pillar height on silicon nanopillar (SiNP) arrays plays a pivotal role in the antibacterial action instead of the SiNP diameter.[50] Interestingly, the authors showed the formation of adhesion bonds over the SiNP points by FIB milling instead of cellular penetration, thus resulting in pillar deformation bending, followed by cell killing in response to bacterial adhesion.[50] Furthermore, Ivanova et al. showed that naturally inspired SiO_2 nanopillars from black silicon generated increased outcomes of antibacterial activity,[51] further supporting that the surface energy and the nanotexture dimensions (height) were the principal parameters of antimicrobial action, rather than the surface chemistry, as observed here. However, an early study of hydrothermally synthesized TiO_2 nanopillars on Ti6Al4V generated antibacterial efficacy against *S. aureus* and *E. coli*.[52] Using the FIB-SEM technology, it was found that the direct contact interaction between the TiO_2 NPs and the bacterial cells induced cellular deformations that subsequently generated cell death by oxidative stress.[52] However, the authors highlighted that the cell envelopment never penetrate the NPs, indicating that the antimicrobial stimulus was mainly due to morphology alterations and deformations in the cell envelope. Furthermore, the fungal cell-wall components can play an essential role in the molecular sensing of the different surface physical parameters to control the attachment and subsequent biofilm formation. Additionally, Pham et al. reported that the major cell-wall components β-1,3-glucan in *C. albicans* facilitate the surface attachment.[53] The authors suggested that the glycan units β-1,6-glucans, β-1,3-glucan-chitin, chitins, and the outer wall elements mannoproteins and mannans may reinforce the adhesion forces to conduct the cell attachment.[53] In addition, the nanoindentation analyses proposed by Pham et al. indicated that the glycan outer wall components could be involved as the principal sensing molecules, which mediate the *C. albicans* adhesion fate.[53] Therefore, our cumulative results are in accordance with the above-proposed mechanisms. Hence, more investigations are recommended to elucidate the molecular pathways of fungal nanoadhesion bond formation and cell-wall deposition on nanotextured materials.

The present work focuses on several fundamental findings that have critical implications for advancing antifungal nanostructured surfaces for biomedical applications. Initially, the transformation from amorphous to anatase showed a higher adhesion and colonization of *C. albicans*. However, our findings point toward a repellent fungal effect instead of a fungicidal issue, as we did not detect substantial outcomes of structural rupture or lysis morphology. Indeed, it is important to highlight that the anatase conducted a promoted fungal extension by increasing the cell envelope insertions into the NTs-annealed, thus, indicating that, for NTs, the antifungal action could not be directly associated to a mechanical disruption, as suggested for different nanostructural topographies.[6,35] Even more, it is important to highlight that fungal cells possess a thicker, more rigid cell wall, resulting in a stiffer membrane.[48,54] Thus, as a proof of concept, we strongly suggest that the fungal adhesion process is mostly conducted by the cellular capability to form nanoadhesion bonds to the material surface instead of cellular disruption by physical events. Another crucial mechanisms identified is that the surface morphology and the crystallographic orientation play a key role in the *C. albicans* reduction, rather than the roughness values. These important physical parameters can account for the rational design of nanostructured antifungal surfaces. Similarly, the wetting behavior of the nanostructured surfaces

https://doi.org/10.1021/acsomega.1c00475
ACS Omega 2021, 6, 15625−15636

could be substantially altered by the fungal environment; however, comprehensive studies are recommended to further elucidate this interesting behavior. In summary, the design of high-aspect-ratio nanostructured surfaces has been documented to effectively disrupt bacterial cells by mechanical rupture during the insertion of bacteria on sharped nanotextured surfaces.[54,55] The physical size and membrane rigidity of typical bacterial cells (Gram-positive and/or -negative) have been considered to be the main factors to conduct cell lysis using nanotextured responsive surfaces.[54,55] However, yeast cells can withstand the torsional stress,[54,56] thus avoiding the fungal insertion by controlling the molecular ordering of nanostructured surfaces. Finally, in Figure 9,a schematic illustration of the reduced fungal adhesion addressed by the amorphous NTs is presented.

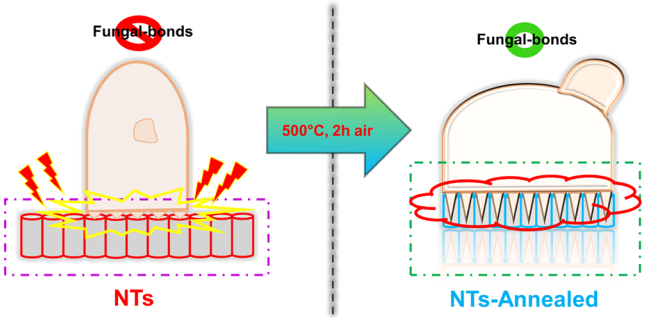

Figure 9. Schematic illustration representing the nanobonding behavior at the fungal−material nanolevel, proposing that annealed NTs conduct cell-envelope penetration (represented by the sharping points); meanwhile, the as-manufactured NTs impede a proper cellular surface connection.

CONCLUSIONS

We have provided evidence of the fungal adhesion behavior on amorphous and anatase NTs transformed by thermal treatment. Considering that anatase is the most widely recommended phase for biomedical applications, we investigated the role of crystallographic orientation on *C. albicans* adhesion. Initially, we developed NTs preserving constant parameters of diameter, roughness, and reduced differences of surface chemistry. The experimental materials showed that NTs are imposed on the cell adhesion, continuing by NTs-annealed and the control Ti6Al4V alloy. Interestingly, the surface energy of the nanostructured materials showed striking alterations under fungal conditions, as depicted by the WCA using *C. albicans*. Moreover, our study elucidated that the surface roughness of anodized TiO_2 nanotubes did not play a predominant role in controlling the adhesion of *C. albicans*, as it has been reported for different nanostructured coatings. However, the crystalline transformation gives rise to cell morphology alterations among the nanotextured specimens, consequently, highlighting significant phenotype differences, which were far relevant to the stimulated development of pseudohyphae, septum formation, and, more importantly, the extended cellular adhesion area stimulated by the anatase NTs. Importantly, our work provides new pieces of evidence with respect to the antifungal mechanism of NTs, which could be strongly mediated by a fungal repellent process instead of mechanical cellular disruption, indicating that the NTs induced evident interruption of fungal nanoadhesion bonds at the biointerface. However, the NTs-annealed further directed the fungal envelope insertion, which might promote the extended area occupied by the cells. Otherwise, the control alloy promoted higher *C. albicans* colonization, supporting the fact that the nanostructured coatings inhibit the fungal growth. The present work focuses on several fundamental findings that have critical implications for advancing antifungal nanostructured surfaces for biomedical applications. Therefore, our current work sheds light on important information of physical parameters that can account for the rational design of nanostructured antifungal surfaces.

MATERIALS AND METHODS

Synthesis of TiO_2 Nanotubes. The NTs were synthesized using our previous established protocol.[30] In brief, Ti6Al4V disks (ASTM F-136, Supra Alloys Inc., Camarillo, CA, USA) of 15 mm diameter and 5 mm thickness were polished by following a metallographic procedure (ASTM E3-11) using SiC emery paper (100−2000 grit) and 0.5 μm alumina to achieve a mirror finish. Next, the samples were cleaned in an ultrasonic bath (Branson, MO, USA) with acetone, ethanol, and distilled water for 30 min each. Then, they were mounted on a flat 125 mL electrochemical cell and anodized using an electrolyte solution prepared with Microdacyn 60 (Oculus technologies, Guadalajara, JAL, MEX), 10 mg/L NH_4F (Sigma-Aldrich, USA), and 100 mg/L NaCl (Sigma-Aldrich, USA) at pH 6.8. Using a dc power supply, a 20 V potential was applied for only 5 min with a platinum mesh as a counter electrode. The anodization was carried out at room temperature (RT). The anodized samples were cleaned in an ultrasonic bath with distilled water for 5 min to eliminate residues of fluoride salts, rinsed with isopropyl alcohol, and dried in a desiccator for 12 h. Aiming to generate anatase phase NTs (NTs-annealed), the anodized samples were placed in a furnace and annealed at 500 °C for 2 h in air with a heating rate of 1 °C min^{-1}. The NT diameter distributions were counted and measured using the Image J software (1.48v, NIH, USA), n = 100. Ti6Al4V samples without any modification were used as control.

Sample Characterization. *Surface Morphology.* To analyze the surface morphology of the experimental substrates, we applied FE-SEM (Tescan LYRA 3, Brno Czech Republic) on random fields at 20 kV accelerating voltage.

Chemical Assessment. The elemental analysis was evaluated by EDX (Bruker, XFlash 6I30) coupled to the FE-SEM, at 10 kV with a large spot size to adjust a suitable count rate per second for spectrum collection.

Surface Topography. The surface topography was studied using AFM (Quesant Q-Scope 350, AMBIOS, Agura Hills, CA, USA), mounted in an antiacoustic box to prevent noise that can affect the measurements. The operation scan rate was 0.5 Hz by the contact mode at RT. A 40 μm $X-Y$ and 4 μm Z scanner equipped with a silicon tip and 10 nm tip curvature was used. The scan surface area was 0.5 for the control and 1 μm^2 for the nanostructured coatings. To compare the roughness differences between the surfaces, we provide the RMS.

Wettability and Surface Energy Measurements. The static WCA of the experimental materials was analyzed by depositing a 5 μL droplet of deionized water at 20 ± 2 °C and 45% relative humidity (RH). The droplet morphology was captured using a high-performance CCD camera of an automatized tensiometer (Theta Attension; Biolin Scientific) equipped with

https://doi.org/10.1021/acsomega.1c00475
ACS Omega 2021, 6, 15625−15636

an $X-Y$ syringe. The WCA values were obtained using the ONE Attension software, which enables a highly precise analysis of the two angles of the drop. The surface energy (ζ) of a material can be calculated from the experimental WCA using the following equation:

$$\zeta = \gamma \cos\theta \quad (1)$$

where γ represents the surface energy between water and air at 20 ± 2 °C (72.8 mJ/m^2) for pure water and θ represent the WCA.[57,58]

XRD Evaluation. The crystalline phase of the as-prepared NTs and the NTs-annealed was explored using a Bruker D8 Advanced diffractometer operated at 30 kV and 30 mA.

C. albicans Culture and Viability Assessment. For the purpose of studying the fungal behavior of the experimental materials as well as the fungal−surface interface, we used a *C. albicans* pathogenic strain isolated from a chronic atrophic oral denture candidiasis patient, as previously described.[7,24] For the fungal culture preparation, discrete colonies of freshly overnight grown *C. albicans* were inoculated in a new Sabouraud Dextrose Broth (SDB, Beckton Dickinson, USA) and grown overnight under standard aerobic conditions. Then, the resulting culture was adjusted to an optical density (O.D.) of 0.034 at 595 nm containing approximately 2 × 10^4 colony-forming units (CFU)/mL, using SDB. Afterward, 50 μL of the prepared *C. albicans* culture plus 100 μL of warmed sterile SDB (to avoid culture dryness) were inoculated on the surfaces of the materials. The samples were incubated under static conditions for 2 and 6 h (defined as the initial and late adhesion phase, respectively) at 37 °C. Then, each substrate was washed three times, with 1× PBS to remove any unbounded cells. Subsequently, each material was transferred to an individual well of a sterile 12-well polystyrene plate (Corning, NY, USA), containing 2 mL of new SDB per well. The 12-well plate was carefully placed in an ultrasonic bath (Branson, MO, USA), sonicated at 120 W for 1 min at intervals of 5 s to prevent cellular lyses, and scraped off using a surgical blade to completely detach any adhered cell. Finally, the materials were aseptically withdrawn, and the remaining suspensions were serially diluted with 1× PBS, cultured in SD agar under standard culture conditions for 24 h, counted for viability quantification, and digitalized in a dark field colony counter (Reichert, NY, USA).

WCA Analysis and ζ Potential of the C. albicans. A solution of double distilled water containing approximately 1 × 10^5 CFU/mL of *C. albicans* was prepared to evaluate the wettability and surface energy behavior of the experimental materials. Briefly, an overnight growing suspension of *C. albicans* was washed three times with 1× PBS by centrifugation at 4500 rpm for 10 min. Next, the resulting washed cellular pellet was adjusted to an O.D. of 0.05 at 595 nm using double distilled water. The WCA with *C. albicans* was then evaluated by placing a 5 μL droplet at 25 ± 2 °C and 45% RH for 10 s using an automatized tensiometer. Likewise, ζ-potential analysis of *C. albicans* was performed using a similarly prepared sample and tested using the NanoTrack Wave II.[14] The data obtained were computed, as indicated above.

FE-SEM Fungal Morphology Analysis. The fungal cell morphology and growth density conducted by the experimental materials under each incubation period were analyzed using high-resolution FE-SEM.[7] In brief, the substrates were individually washed with warm 1× PBS three times for 5 min, fixed with 3% glutaraldehyde (Sigma-Aldrich, St. Louis, MI, USA) at 4°C overnight, washed three times with PBS, and postfixed with 3% glutaraldehyde solution for 2 h at RT. Subsequently, the samples were dehydrated in graded series of ethanol solutions (2 h, each) at RT and incubated in absolute ethanol for 24 h at 4 °C.

Surface−Fungal Interface by FIB. For the characterization of the fungal−surface interface at the initial (2 h) adhesion period, the experimental samples were prepared for FE-SEM, as described above. Then, the FIB (coupled with the FE-SEM) was applied for cross sectioning the adhered cells, and the connecting nanoadhesion bonds were visualized at high-zoom magnifications.[24] The magnifications applied were 50 000× and 100 000×, operating at 10 kV and a working distance of 9.00 mm. The FIB operation parameters were at 100 pA and a beam diameter of 3 nm at 17 kV. Importantly, the fixed cells were not sputter coated to evade the nanostructured interface coverage at a very high magnification scale.

Statistical Analysis. The numerical information from the experimental results was analyzed by one-way analysis of variances followed by Tukey's multiple comparison test when appropriate. Data were expressed as the mean ± standard deviation of three independent experiments performed each in triplicate. A $p < 0.05$ was considered statistically significant. GraphPad Prism 7 software (GraphPad Inc., USA) was used as the statistical package.

■ ASSOCIATED CONTENT

Supporting Information

The Supporting Information is available free of charge at https://pubs.acs.org/doi/10.1021/acsomega.1c00475.

3D AFM characterization of the nanostructured materials (Figure S1), contact angles of active *C. albicans* on the surfaces (Figure S2), high-magnification FE-SEM detailing the yeast phenotype on the experimental surfaces (Figure S3), and EDX elemental analysis (Table S1) (PDF)

■ AUTHOR INFORMATION

Corresponding Authors

Ernesto Beltrán-Partida − *Laboratorio de Biología Molecular y Cáncer, Instituto de Ingeniería, Universidad Autónoma de Baja California, Mexicali, Baja California C.P. 21280, México; Laboratorio de Corrosión y Materiales Avanzados, Instituto de Ingeniería, Universidad Autónoma de Baja California, Mexicali, Baja California C. P. 21280, México*; Email: beltrane@uabc.edu.mx

Benjamín Valdez-Salas − *Laboratorio de Biología Molecular y Cáncer, Instituto de Ingeniería, Universidad Autónoma de Baja California, Mexicali, Baja California C.P. 21280, México; Laboratorio de Corrosión y Materiales Avanzados, Instituto de Ingeniería, Universidad Autónoma de Baja California, Mexicali, Baja California C. P. 21280, México*; Email: benval@uabc.edu.mx; Fax: +52-686-5664150

Authors

Mario Curiel-Álvarez − *Laboratorio de Corrosión y Materiales Avanzados, Instituto de Ingeniería, Universidad Autónoma de Baja California, Mexicali, Baja California C. P. 21280, México*

Minerva Guerra-Balcázar − *Facultad de Ingeniería, División de Investigación y Posgrado, Universidad Autónoma de Querétaro, Querétaro C. P. 76010, México*

https://doi.org/10.1021/acsomega.1c00475
ACS Omega 2021, 6, 15625−15636

Noé Arjona − *Centro de Investigación y Desarrollo Tecnológico en Electroquímica S. C., Querétaro C. P. 76703, México;* orcid.org/0000-0002-4136-4738

Complete contact information is available at: https://pubs.acs.org/10.1021/acsomega.1c00475

Notes

The authors declare no competing financial interest.

■ ACKNOWLEDGMENTS

The authors wish to thank the program no. A1-S-38368, "Proyecto Apoyado por el Fondo Sectorial de Investigación para la Educación" CB2017-2018, SEP-CONACYT, for financial support.

■ REFERENCES

(1) Vera-González, N.; Shukla, A. Advances in Biomaterials for the Prevention and Disruption of Candida Biofilms. *Front. Microbiol.* **2020**, *11*, 2251.

(2) Lee, S. W.; Phillips, K. S.; Gu, H.; Kazemzadeh-Narbat, M.; Ren, D. How microbes read the map: Effects of implant topography on bacterial adhesion and biofilm formation. *Biomaterials* **2021**, *268*, No. 120595.

(3) Huang, D.-N.; Wang, J.; Ren, K.-F.; Ji, J. Functionalized biomaterials to combat biofilms. *Biomater. Sci.* **2020**, *8*, 4052−4066.

(4) Lee, S. W.; Gu, H.; Kilberg, J. B.; Ren, D. Sensitizing bacterial cells to antibiotics by shape recovery triggered biofilm dispersion. *Acta Biomater.* **2018**, *81*, 93−102.

(5) Karygianni, L.; Ren, Z.; Koo, H.; Thurnheer, T. Biofilm Matrixome: Extracellular Components in Structured Microbial Communities. *Trends Microbiol.* **2020**, *28*, 668−681.

(6) Le, P. H.; Nguyen, D. H. K.; Aburto-Medina, A.; Linklater, D. P.; Crawford, R. J.; MacLaughlin, S.; Ivanova, E. P. Nanoscale Surface Roughness Influences Candida albicans Biofilm Formation. *ACS Appl. Bio Mater.* **2020**, *3*, 8581−8591.

(7) Valdez-Salas, B.; Beltrán-Partida, E.; Nedev, N.; Ibarra-Wiley, R.; Salinas, R.; Curiel-Álvarez, M.; Valenzuela-Ontiveros, Y.; Pérez, G. Controlled antifungal behavior on Ti6Al4V nanostructured by chemical nanopatterning. *Mater. Sci. Eng., C* **2019**, *96*, 677−683.

(8) Dunn, M. J.; Fillinger, R. J.; Anderson, L. M.; Anderson, M. Z. Automated quantification of Candida albicans biofilm-related phenotypes reveals additive contributions to biofilm production. *Npj Biofilms Microbiomes* **2020**, *6*, No. 36.

(9) Spettel, K.; Barousch, W.; Makristathis, A.; Zeller, I.; Nehr, M.; Selitsch, B.; Lackner, M.; Rath, P.-M.; Steinmann, J.; Willinger, B. Analysis of antifungal resistance genes in Candida albicans and Candida glabrata using next generation sequencing. *PLoS One* **2019**, *14*, No. e0210397.

(10) Lohse, M. B.; Gulati, M.; Johnson, A. D.; Nobile, C. J. Development and regulation of single- and multi-species Candida albicans biofilms. *Nat. Rev. Microbiol.* **2018**, *16*, 19−31.

(11) Lüdecke, C.; Roth, M.; Yu, W.; Horn, U.; Bossert, J.; Jandt, K. D. Nanorough titanium surfaces reduce adhesion of *Escherichia coli* and *Staphylococcus aureus* via nano adhesion points. *Colloids Surf., B* **2016**, *145*, 617−625.

(12) Valdez-Salas, B.; Beltrán-Partida, E.; Castillo-Uribe, S.; Curiel-Álvarez, M.; Zlatev, R.; Stoytcheva, M.; Montero-Alpírez, G.; Vargas-Osuna, L. In Vitro Assessment of Early Bacterial Activity on Micro/Nanostructured Ti6Al4V Surfaces. *Molecules* **2017**, *22*, 832.

(13) Cloutier, M.; Mantovani, D.; Rosei, F. Antibacterial Coatings: Challenges, Perspectives, and Opportunities. *Trends Biotechnol.* **2015**, *33*, 637−652.

(14) Valdez-Salas, B.; Beltrán-Partida, E.; Zlatev, R.; Stoytcheva, M.; Gonzalez-Mendoza, D.; Salvador-Carlos, J.; Moreno-Ulloa, A.; Cheng, N. Structure-activity relationship of diameter controlled Ag@Cu nanoparticles in broad-spectrum antibacterial mechanism. *Mater. Sci. Eng., C* **2021**, *119*, No. 111501.

(15) Song, R.; Zhang, Y.; Huang, Q.; Yang, Y.; Lin, L.; Liang, J.; Hu, R.; Rui, G.; Lin, C. Facile Construction of Structural Gradient of TiO2 Nanotube Arrays on Medical Titanium for High Throughput Evaluation of Biocompatibility and Antibacterial Property. *ACS Appl. Bio Mater.* **2018**, *1*, 1056−1065.

(16) Yan, Y.; Soraru, C.; Keller, V.; Keller, N.; Ploux, L. Antibacterial and Biofilm-Preventive Photocatalytic Activity and Mechanisms on P/F-Modified TiO2 Coatings. *ACS Appl. Bio Mater.* **2020**, *3*, 5687−5698.

(17) Beltrán-Partida, E.; Valdez-Salas, B.; Escamilla, A.; Moreno-Ulloa, A.; Burtseva, L.; Valdez-Salas, E.; Curiel Alvarez, M.; Nedev, N. The Promotion of Antibacterial Effects of Ti6Al4V Alloy Modified with TiO_2 Nanotubes Using a Superoxidized Solution. *J. Nanomater.* **2015**, *2015*, No. 818565.

(18) Li, X.; Wang, B.; Zhou, S.; Chen, W.; Chen, H.; Liang, S.; Zheng, L.; Yu, H.; Chu, R.; Wang, M.; Chai, Z.; Feng, W. Surface chemistry governs the sub-organ transfer, clearance and toxicity of functional gold nanoparticles in the liver and kidney. *J. Nanobiotechnol.* **2020**, *18*, 45.

(19) Rasouli, R.; Barhoum, A.; Uludag, H. A review of nanostructured surfaces and materials for dental implants: Surface coating, patterning and functionalization for improved performance. *Biomater. Sci.* **2018**, *6*, 1312−1338.

(20) Khalid, S.; Gao, A.; Wang, G.; Chu, P. K.; Wang, H. Tuning surface topographies on biomaterials to control bacterial infection. *Biomater. Sci.* **2020**, *8*, 6840−6857.

(21) Williams, D. F. Biocompatibility Pathways: Biomaterials-Induced Sterile Inflammation, Mechanotransduction, and Principles of Biocompatibility Control. *ACS Biomater. Sci. Eng.* **2017**, *3*, 2−35.

(22) Makvandi, P.; Ghomi, M.; Padil, V. V. T.; Shalchy, F.; Ashrafizadeh, M.; Askarinejad, S.; Pourreza, N.; Zarrabi, A.; Nazarzadeh Zare, E.; Kooti, M.; Mokhtari, B.; Borzacchiello, A.; Tay, F. R. Biofabricated Nanostructures and Their Composites in Regenerative Medicine. *ACS Appl. Nano Mater.* **2020**, *3*, 6210−6238.

(23) Gaharwar, A. K.; Singh, I.; Khademhosseini, A. Engineered biomaterials for in situ tissue regeneration. *Nat. Rev. Mater.* **2020**, *5*, 686−705.

(24) Beltrán-Partida, E.; Valdez-Salas, B.; Curiel-Álvarez, M.; Castillo-Uribe, S.; Escamilla, A.; Nedev, N. Enhanced antifungal activity by disinfected titanium dioxide nanotubes via reduced nano-adhesion bonds. *Mater. Sci. Eng., C* **2017**, *76*, 59−65.

(25) Dewald, C.; Lüdecke, C.; Firkowska-Boden, I.; Roth, M.; Bossert, J.; Jandt, K. D. Gold nanoparticle contact point density controls microbial adhesion on gold surfaces. *Colloids Surf., B* **2018**, *163*, 201−208.

(26) Brammer, K. S.; Frandsen, C. J.; Jin, S. TiO2 nanotubes for bone regeneration. *Trends Biotechnol.* **2012**, *30*, 315−322.

(27) Shi, X.; Xu, Q.; Tian, A.; Tian, Y.; Xue, X.; Sun, H.; Yang, H.; Dong, C. Antibacterial activities of TiO2 nanotubes on *Porphyromonas gingivalis*. *RSC Adv.* **2015**, *5*, 34237−34242.

(28) Li, H.; Cui, Q.; Feng, B.; Wang, J.; Lu, X.; Weng, J. Antibacterial activity of TiO2 nanotubes: Influence of crystal phase, morphology and Ag deposition. *Appl. Surf. Sci.* **2013**, *284*, 179−183.

(29) Chouirfa, H.; Bouloussa, H.; Migonney, V.; Falentin-Daudré, C. Review of titanium surface modification techniques and coatings for antibacterial applications. *Acta Biomater.* **2019**, *83*, 37−54.

(30) Beltrán-Partida, E.; Valdez-Salas, B.; Escamilla, A.; Curiel, M.; Valdez-Salas, E.; Nedev, N.; Bastidas, J. M. Disinfection of titanium dioxide nanotubes using super-oxidized water decrease bacterial viability without disrupting osteoblast behavior. *Mater. Sci. Eng., C* **2016**, *60*, 239−245.

(31) Ercan, B.; Taylor, E.; Alpaslan, E.; Webster, T. J. Diameter of titanium nanotubes influences anti-bacterial efficacy. *Nanotechnology* **2011**, *22*, No. 295102.

(32) Harriott, M. M.; Noverr, M. C. Importance of Candida−bacterial polymicrobial biofilms in disease. *Trends Microbiol.* **2011**, *19*, 557−563.

(33) Linklater, D. P.; Juodkazis, S.; Ivanova, E. P. Nanofabrication of mechano-bactericidal surfaces. *Nanoscale* **2017**, *9*, 16564−16585.

(34) Bhadra, C. M.; Khanh Truong, V.; Pham, V. T. H.; Al Kobaisi, M.; Seniutinas, G.; Wang, J. Y.; Juodkazis, S.; Crawford, R. J.; Ivanova, E. P. Antibacterial titanium nano-patterned arrays inspired by dragonfly wings. *Sci. Rep.* **2015**, *5*, No. 16817.
(35) Linklater, D. P.; Baulin, V. A.; Juodkazis, S.; Crawford, R. J.; Stoodley, P.; Ivanova, E. P. Mechano-bactericidal actions of nanostructured surfaces. *Nat. Rev. Microbiol.* **2021**, *19*, 8−22.
(36) Ghilini, F.; Pissinis, D. E.; Miñán, A.; Schilardi, P. L.; Diaz, C. How Functionalized Surfaces Can Inhibit Bacterial Adhesion and Viability. *ACS Biomater. Sci. Eng.* **2019**, *5*, 4920−4936.
(37) Civantos, A.; Martínez-Campos, E.; Ramos, V.; Elvira, C.; Gallardo, A.; Abarrategi, A. Titanium Coatings and Surface Modifications: Toward Clinically Useful Bioactive Implants. *ACS Biomater. Sci. Eng.* **2017**, *3*, 1245−1261.
(38) Perez-Jorge, C.; Arenas, M.-A.; Conde, A.; Hernández-Lopez, J.-M.; De Damborenea, J.-J.; Fisher, S.; Hunt, A. M. A.; Esteban, J.; James, G. Bacterial and fungal biofilm formation on anodized titanium alloys with fluorine. *J. Mater. Sci.: Mater. Med.* **2017**, *28*, No. 8.
(39) Pérez-Jorge, C.; Conde, A.; Arenas, M. A.; Pérez-Tanoira, R.; Matykina, E.; De Damborenea, J. J.; Gómez-Barrena, E.; Esteban, J. In vitro assessment of *Staphylococcus epidermidis* and *Staphylococcus aureus* adhesion on TiO2 nanotubes on Ti−6Al−4V alloy. *J. Biomed. Mater. Res., Part A* **2012**, *100A*, 1696−1705.
(40) Hasan, J.; Crawford, R. J.; Ivanova, E. P. Antibacterial surfaces: The quest for a new generation of biomaterials. *Trends Biotechnol.* **2013**, *31*, 295−304.
(41) Almaguer-Flores, A.; Silva-Bermudez, P.; Galicia, R.; Rodil, S. E. Bacterial adhesion on amorphous and crystalline metal oxide coatings. *Mater. Sci. Eng., C* **2015**, *57*, 88−99.
(42) Gallardo-Moreno, A. M.; Pacha-Olivenza, M. A.; Fernández-Calderón, M.-C.; Pérez-Giraldo, C.; Bruque, J. M.; González-Martín, M.-L. Bactericidal behaviour of Ti6Al4V surfaces after exposure to UV-C light. *Biomaterials* **2010**, *31*, 5159−5168.
(43) Regonini, D.; Bowen, C. R.; Jaroenworaluck, A.; Stevens, R. A review of growth mechanism, structure and crystallinity of anodized TiO2 nanotubes. *Mater. Sci. Eng., R* **2013**, *74*, 377−406.
(44) Paramasivam, I.; Jha, H.; Liu, N.; Schmuki, P. A Review of Photocatalysis using Self-organized TiO2 Nanotubes and Other Ordered Oxide Nanostructures. *Small* **2012**, *8*, 3073−3103.
(45) Kondo, J. N.; Domen, K. Crystallization of Mesoporous Metal Oxides. *Chem. Mater.* **2008**, *20*, 835−847.
(46) Gongadze, E.; Kabaso, D.; Bauer, S.; Slivnik, T.; Schmuki, P.; Van Rienen, U.; Iglič, A. Adhesion of osteoblasts to a nanorough titanium implant surface. *Int. J. Nanomed.* **2011**, *6*, 1801−1816.
(47) Liu, N.; Paramasivam, I.; Yang, M.; Schmuki, P. Some critical factors for photocatalysis on self-organized TiO2 nanotubes. *J. Solid State Electrochem.* **2012**, *16*, 3499−3504.
(48) Elbourne, A.; Cheeseman, S.; Wainer, P.; Kim, J.; Medvedev, A. E.; Boyce, K. J.; McConville, C. F.; Van Embden, J.; Crawford, R. J.; Chapman, J.; Truong, V. K.; Della Gaspera, E. Significant Enhancement of Antimicrobial Activity in Oxygen-Deficient Zinc Oxide Nanowires. *ACS Appl. Bio Mater.* **2020**, *3*, 2997−3004.
(49) Nowlin, K.; Boseman, A.; Covell, A.; LaJeunesse, D. Adhesion-dependent rupturing of Saccharomyces cerevisiae on biological antimicrobial nanostructured surfaces. *J. R. Soc., Interface* **2015**, *12*, No. 20140999.
(50) Ivanova, E. P.; Linklater, D. P.; Werner, M.; Baulin, V. A.; Xu, X.; Vrancken, N.; Rubanov, S.; Hanssen, E.; Wandiyanto, J.; Truong, V. K.; Elbourne, A.; Maclaughlin, S.; Juodkazis, S.; Crawford, R. J. The multi-faceted mechano-bactericidal mechanism of nanostructured surfaces. *Proc. Nat. Acad. Sci. U. S. A* **2020**, *117*, 12598−12605.
(51) Ivanova, E. P.; Hasan, J.; Webb, H. K.; Gervinskas, G.; Juodkazis, S.; Truong, V. K.; Wu, A. H. F.; Lamb, R. N.; Baulin, V. A.; Watson, G. S.; Watson, J. A.; Mainwaring, D. E.; Crawford, R. J. Bactericidal activity of black silicon. *Nat. Commun.* **2013**, *4*, No. 2838.
(52) Jenkins, J.; Mantell, J.; Neal, C.; Gholinia, A.; Verkade, P.; Nobbs, A. H.; Su, B. Antibacterial effects of nanopillar surfaces are mediated by cell impedance, penetration and induction of oxidative stress. *Nat. Commun.* **2020**, *11*, No. 1626.
(53) Pham, D. Q.; Bryant, S. J.; Cheeseman, S.; Huang, L. Z. Y.; Bryant, G.; Dupont, M. F.; Chapman, J.; Berndt, C. C.; Vongsvivut, J.; Crawford, R. J.; Truong, V. K.; Ang, A. S. M.; Elbourne, A. Micro- to nano-scale chemical and mechanical mapping of antimicrobial-resistant fungal biofilms. *Nanoscale* **2020**, *12*, 19888−19904.
(54) Elbourne, A.; Chapman, J.; Gelmi, A.; Cozzolino, D.; Crawford, R. J.; Truong, V. K. Bacterial-nanostructure interactions: The role of cell elasticity and adhesion forces. *J. Colloid Interface Sci.* **2019**, *546*, 192−210.
(55) Elbourne, A.; Crawford, R. J.; Ivanova, E. P. Nano-structured antimicrobial surfaces: From nature to synthetic analogues. *J. Colloid Interface Sci.* **2017**, *508*, 603−616.
(56) Pham, V. T. H.; Truong, V. K.; Mainwaring, D. E.; Guo, Y.; Baulin, V. A.; Al Kobaisi, M.; Gervinskas, G.; Juodkazis, S.; Zeng, W. R.; Doran, P. P.; Crawford, R. J.; Ivanova, E. P. Nanotopography as a trigger for the microscale, autogenous and passive lysis of erythrocytes. *J. Mater. Chem. B* **2014**, *2*, 2819−2826.
(57) Liu, X.; Lim, J. Y.; Donahue, H. J.; Dhurjati, R.; Mastro, A. M.; Vogler, E. A. Influence of substratum surface chemistry/energy and topography on the human fetal osteoblastic cell line hFOB 1.19: Phenotypic and genotypic responses observed in vitro. *Biomaterials* **2007**, *28*, 4535−4550.
(58) Mazare, A.; Totea, G.; Burnei, C.; Schmuki, P.; Demetrescu, I.; Ionita, D. Corrosion, antibacterial activity and haemocompatibility of TiO2 nanotubes as a function of their annealing temperature. *Corros. Sci.* **2016**, *103*, 215−222.

https://doi.org/10.1021/acsomega.1c00475
ACS Omega 2021, 6, 15625−15636